Solar Energy 135 (2016) 215–221

Contents lists available at ScienceDirect

Solar Energy

journal homepage: www.elsevier.com/locate/solener

Characterization of recombination properties at diffused surfaces for industrial silicon solar cell concepts

Md. Momtazur Rahman [a,*], Hasan Mahamudul [b], Md. Nazmul Hasan [c]

[a] University of Ulm, Helmholtzstraße 18, 89081 Ulm, Germany
[b] University of Malaya, Kuala Lumpur 50670, Malaysia
[c] National Cheng Kung University, Tainan City 701, Taiwan

ARTICLE INFO

Article history:
Received 10 November 2015
Received in revised form 9 May 2016
Accepted 25 May 2016

Keywords:
Emitter formation
Passivation technique
Recombination properties
Monocrystalline silicon solar cell

ABSTRACT

This paper describes an experiment to evaluate the surface recombination properties of phosphorous diffused surfaces for crystalline silicon solar cells. In this experiment the analysis of surface recombination properties for the phosphoryl chloride ($POCl_3$) diffusion is carried out. Investigation of recombination properties on diffused surfaces is crucial for the conversion efficiency of silicon solar cells. Hence, the dark saturation current densities (J_o) are determined via quasi steady state photoconductance (QSSPC) decay measurement and the doping profiles by electrochemical-capacitance voltage (ECV) measurement. All the diffusion processes are performed in a quartz tube furnace. The samples are diffused at peak temperatures of 800–950 °C. Therefore; the influence of several parameters for example the extent of surface concentration, the diffusion temperature and the dark saturation current density (J_o) are evaluated.

1. Introduction

Solar energy is one of the promising energy sources among all the available energy sources in the earth. Basically, this technology works on the principle of photovoltaic (PV) and the term 'photovoltaic' refers to direct conversion of sunlight into electricity. Various types of losses normally occur in the solar cell; those losses effectively limit its electrical parameters and thus the energy conversion efficiency. Researchers are devoted to reduce those losses in order to increase the cell efficiency.

The price for converting solar energy into electricity is significantly reduced with the immense advancement of PV production technology and is expected to maintain relatively high share in the future energy supply. Although, the price is not still competitive in comparison with the conventional energy sources, so the price reduction is essential. The photovoltaic industry intends to reduce the peak cost of solar cells. This can be implemented effectively by reducing the supplementary costs while developing efficient solar cell. One of the key factors to improve the cell efficiency is to reduce the recombination losses at the surface, for example optimizing the passivation layer on both surfaces or reduce the doping concentration at the front surface.

For the case of the aluminum back surface field (Al-BSF) solar cell (cell technology that has the highest share of the market), different types of losses are encountered. For high-quality base material, those losses are mainly located at the surfaces. Optical and electrical losses are due to the reflection of incident photons from top of the surface and the series resistance of the cell. These optical and electrical losses are contributing to reduce the cell efficiency. Also the concentration of defect centers may be caused by oxygen atoms, metallic impurities or crystal lattice dislocations during the wafer processing which limits the efficiency of solar cells (Powell et al., 2012).

Most manufacturers fabricate *p*-type wafers as a base and *n*-type diffused layer as an emitter. So, optimization of *n*-type diffused layer resistance is essential; since the aim is to obtain high doping below the contact interface to reduce the contact resistance, as usual to reduce the electrical losses at the front surface. Basically diffused surfaces are applied in a silicon solar cell to form an emitter. The intention is to collect or separate the photogenerated carriers, or to reduce the recombination rate at the metal–semiconductor interface. For quality considerations, it is necessary to reduce the surface recombination by decreasing the defect concentrations at the surface, which can be done by effective surface passivation. There are two strategies for reducing the recombination velocity at the surface: chemical passivation and field effect passivation.

* Corresponding author.
E-mail address: md.momtazur.rahman@outlook.com (M.M. Rahman).

http://dx.doi.org/10.1016/j.solener.2016.05.042
0038-092X/

In the past years, new metallization materials for the front-side of crystalline silicon solar cells entered the market reaching low resistive contacts to a broad range of surface doping concentrations. Furthermore, several new solar cell concepts enter the market, each featuring specific requirements for the surface near doping of the wafer. This development increased the need for optimization of the doping profiles (Durán et al., 1991) and thus increases the complexity of the doping processes. For further optimization, simulation of the recombination properties of such surface-near doping is beneficial.

For the simulation of the recombination properties of phosphorus doped surfaces, the surface recombination velocity (SRV) in dependence of the surface doping density has to be known for a given passivation technique.

The surface recombination velocity (SRV) can be calculated from the doping profile and the corresponding dark saturation current density of the passivated surface (Cuevas et al., 1993). The aim of this work is to obtain such data-sets for three different industrially applied passivation techniques and a broad range of phosphorus surface concentrations. The data-sets can be used to evaluate doping-dependent surface recombination velocities (SRV).

2. Recombination mechanisms

Illumination of the semiconductor with enough high energy photons ($h\nu > E_g$) leads to the transition of electrons (e^-) from respective valence band to the conduction band. This process is called photo-generation, described by the local generation rate $G(t,x)$, as defined by the density of generated carriers per unit time (Stangl et al., 2010). The reverse of this process is called recombination, described by the local recombination rate $R(t,x)$, as defined by the density of recombining carriers per unit time. The recombination activity is usually described by the carrier lifetime τ, defined as the half lifetime of Δn over time, when no generation or additional recombination is present. It can be expressed with the recombination rate via $\tau = \frac{\Delta n}{U}$. Here Δn, is the excess minority carrier concentration. A significant parameter in a solar cell is the rate at which the recombination occurs. Such a process is known as the recombination rate (U). That rate mainly depends on the number of excess minority carriers.

2.1. Recombination via surface states

The surface recombination plays an important role in determining the solar cell performance. Typically the surface recombination complicates the measurement of bulk lifetime (Sproul, 1994). Since the surface contains dangling bonds or disruption of the crystalline structure, the defects or impurities at the surface promote this recombination. Due to this, the minority carrier lifetime is reduced in the vicinity of the surface.

A parameter called effective surface recombination velocity S_{eff} is used to specify the recombination rate in the surface and is applied to obtain the recombination current J_{rec} (current resulting from the flow of electron and holes pairs that recombine in the space charge region of the forward biased p–n junction) at a given surface, as follows (Kane and Swanson, 1985);

$$J_{rec} = qS_{eff}\Delta n \tag{1}$$

Here, q is the electron charge. The surface recombination of a given sample can be defined analogously to the recombination in the bulk ($\frac{1}{\tau_{bulk}} = \frac{1}{\tau_{rad}} + \frac{1}{\tau_{Auger}} + \frac{1}{\tau_{SRH}}$). Consequently; this surface lifetime τ_s leads to the effective carrier lifetime.

$$\frac{I}{\tau_{eff}} = \frac{I}{\tau_{bulk}} + \frac{I}{\tau_s} = \frac{I}{\tau_{rad}} + \frac{I}{\tau_{Auger}} + \frac{I}{\tau_{SRH}} + \frac{I}{\tau_s} = \frac{1}{\tau_{int}} + \frac{I}{\tau_{SRH}} + \frac{I}{\tau_s} \tag{2}$$

where the intrinsic recombination lifetime (τ_{int}) can be defined as a result of the radiative and Auger recombination lifetime.

Basically; if the diffusion length L is higher than the path the electron needs to diffuse in order to reach the emitter, then the electron can reach this region, otherwise it will recombine in the base. This behavior is related to the effective lifetime and diffusivity as follows;

$$L = \sqrt{D\tau_{eff}} \tag{3}$$

Surface lifetime can be calculated as a function of surface recombination velocity (Luke and Cheng, 1987) (S_1 and S_2), wafer thickness W and the minority carrier diffusion coefficient D (m^2/s), this can be comprehended from Fig. 1.

The following section is described in detail by Baruch et al. (1995). Sproul calculates the surface lifetime for a given sample assuming that generation has stopped after becoming spatially homogeneous. For a symmetrical sample ($S = S_1 = S_2$), the surface lifetime can be expressed as follows;

$$\tau_S = \frac{W}{2S} + \frac{1}{D}\left(\frac{W}{\pi}\right)^2 \tag{4}$$

Hence lifetime becomes $\tau_S = \frac{W}{2S}$. This signifies that diffusivity does not play a role and the excess carriers are spatially homogenously distributed. For infinite surface recombination, τ_S becomes independent from S, meaning that the lifetime is limited by how fast the carriers diffuse towards the surface.

When the rear surface is perfectly passivated means that $S_1 = 0$ (one surface is passivated) it follows;

$$\tau_S = \frac{W}{S_1} + \frac{4}{D}\left(\frac{W}{\pi}\right)^2 \tag{5}$$

The photo current can be reduced by the emitter, for example when carriers are created in the emitter do recombine there and thus do not reach the p–n-junction. In this way the emitter serves as an optical filter, which should be avoided. These losses are reduced by shallow emitter (less generation in the emitter, shorter distance to p–n-junction), low doping densities (longer diffusion length in the emitter) and good surface passivation.

The dark saturation current density of the emitter is a function of the recombination within the emitter. There exists an accurate analytical description of J_o in literature (Cuevas et al., 1993). First order J_o can be described as the surface recombination current at the emitter surface in equilibrium state;

$$J_o^{oth} = qS_P p_o(W) \tag{6}$$

Here S_P denotes the surface recombination velocity at the emitter surface and p_o the hole concentration at equilibrium. The spatial variable perpendicular to the surface is called x, being 0 at the

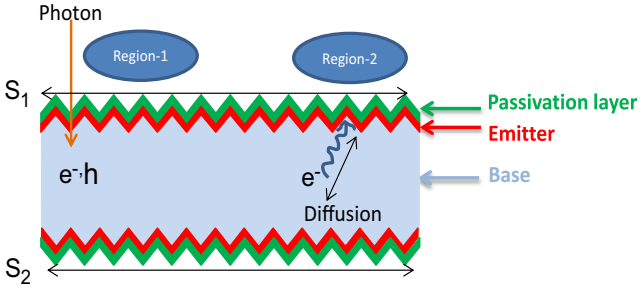

Fig. 1. Schematic diagram of a diffused and passivated wafer, including a front and back surface recombination velocity (S_1 and S_2). Here, region-1 and region-2 respectively represents the electron-hole pair's generation and diffusion towards the emitter.

space-charge region and W at the surface. For higher orders, other effects take place: the Auger-recombination in the emitter here denoted as τ_p and shielding of the surface by means of finite carrier diffusion with the diffusion coefficient D_p, in third order J_o is;

$$J_o^{3rd} = q\frac{S_P p_o(W)(1+B_2)+\overline{A_1}+\overline{A_3}}{1+\overline{B_2}+S_P p_o(W)(A_1+A_3)}$$
$$A_1(W) = \int_0^W \frac{dx}{D_p(x)p_0(x)}$$
$$\overline{A_1}(W) = \int_0^W \frac{p_0(x)}{\tau_p(x)}dx$$
$$B_2(W) = \int_0^W \frac{\overline{A_1}(x)}{D_p(x)p_0(x)}dx \quad (7)$$
$$\overline{B_2}(W) = \int_0^W A_1(x)\frac{p_0(x)}{\tau_p(x)}dx$$
$$A_3(W) = \int_0^W \frac{\overline{B_2}(X)}{D_p(x)p_0(x)}dx$$
$$\overline{A_3}(W) = \int_0^W B_2(x)\frac{p_0(x)}{\tau_p(x)}dx$$

Overall it can be stated that J_o decreases with decreasing doping density for the following reasons: the Auger-recombination decreases in the bulk of the emitter and the SRV decreases with decreasing surface doping concentration. On the other hand, below the metal contacts the SRV is very high – thus to reach a low J_o there, high doping concentrations leading to a low diffusion coefficients and deep profiles are beneficial. According to the one-diode model, J_o is limiting the output voltage of the solar cell (Baruch et al., 1995).

From the previous paragraph, it can be concluded that the regions under the contacts should be heavily doped while the emitter doping should be controlled by the trade-offs between achieving a low emitter dark saturation current density and maintaining a high emitter conductivity. Depending on the metallization technique and the contact formation on the emitter surfaces, the series resistance needs to account for optimum current flow, as the fill factor (*FF*) decreases with increasing series resistance.

The remainder of the paper is organized as follows: Steady state photo conductance (QSSPC) technique, simplified the equation of dark saturation current densities and how to obtain the minority carrier lifetime, and calculation of emitter dark saturation current density (J_o) for both planar and textured surfaces are presented in Section 3. The experimental approach & procedure has been shown in Section 4. The results of diffused samples including the data comparison and newly obtained data application and its challenges for facing the widespread deployment of diffused solar cell and vision for future research in this area are discussed in Section 5. QSSPC measurement results including its recombination properties analysis are discussed in Section 6. Section 7 concludes the paper.

3. QSSPC measurement techniques

The quasi steady state photo conductance (QSSPC) technique is widely used for minority carrier lifetime measurement. This instrument gives the option to examine recombination processes at the passivated surface. Basically, optical methods are used in this instrument to generate excess charge carriers while measuring the effective lifetime. For that, a simple photographic Xenon flash lamp is used (Sinton Instrument, 2011; Sze, 1981; Nagel et al., 1999).

3.1. Dark saturation current density (J_o) analysis

The recombination process occurring in the emitter is complex. However, due to its high doping concentrations the emitter is always under low injection conditions for the considered cases. Thus, the recombination properties (carrier lifetimes) in the emitter are independent from injection level. The recombination current at the base side of the p–n-junction can be expressed as (Kerr et al., 2002);

$$J_{rec} = J_0\frac{np}{n_i^2} \quad (8)$$

Here J_0 is defined as the emitter dark saturation current density, n_i is the intrinsic carrier concentration, and n, p are the electron and hole concentration, respectively.

Combining Eqs. (8) and (1) gives;

$$S_{eff}\ \Delta n = \frac{J_{rec}}{q} = J_0\frac{np}{n_i^2} \quad (9)$$

In which S_{eff} represent the effective surface recombination velocity. Considering a p-type substrate, the previous equation can be simplified to;

$$S_{eff} = J_0\frac{N_A+\Delta n}{qn_i^2} \quad (10)$$

The above equation is known as the quasi static emitter approximation (Kane and Swanson, 1985). Here, N_A is the concentration of the acceptor atoms and q is the electron charge. For symmetrical lifetime samples, the effective surface recombination can be obtained by considering the sample thickness as follows from Eq. (4) Sproul, 1994;

$$S_{eff} = \frac{W}{2}\left[\tau_S - \frac{W^2}{D\pi^2}\right] \quad (11)$$

Here τ_S represents the surface lifetime and D is the diffusivity (m^2/s). Deriving Eq. (10) for Δn leads to;

$$J_0 = q\frac{d}{d\Delta n}(S_{eff}n_i^2) \quad (12)$$

Basically, intrinsic recombination is a material property and depends only on the carrier concentration, so the intrinsic lifetime effect is subtracted from the effective lifetime in order to analyze the dark saturation current density and use the Auger-corrected lifetime as follows;

$$\frac{1}{\tau_{corr}} = \frac{1}{\tau_{eff}} - \frac{1}{\tau_{int}} \quad (13)$$

Then surface lifetime from Eqs. (2) and (13) leads to;

$$\frac{1}{\tau_s} = \frac{1}{\tau_{corr}} - \frac{1}{\tau_{SRH}} \quad (14)$$

For the symmetrical sample (which has been diffused and passivated at both sides), together with Eq. (11), neglecting the diffusion term on the right hand side $\left(\frac{W^2}{D\pi^2}\right)$ (assuming a spatially uniform injection density) and then putting τ_s from Eq. (14), leads to Kane and Swanson, 1985;

$$J_0 = \frac{qW}{2}\frac{d}{d\Delta n}\left(\frac{n_i^2}{\tau_s}\right) = \frac{qW}{2}\frac{d}{d\Delta n}\left(\frac{n_{i^2}}{\tau_{corr}} - \frac{n_{i^2}}{\tau_{SRH}}\right) \quad (15)$$

Eq. (15) is only valid when the bulk lifetime is sufficiently high to allow generated carriers to reach both surfaces and when J_0 is sufficiently low to avoid transport-limited profiles near the surface.

Moreover, injecting carriers into a substrate leads to the band gap narrowing, therefore effective intrinsic carrier concentration n_i is not independent from excess carrier concentration Δn. Since τ_{SRH} is not known, the following condition has to be fulfilled;

$$\frac{d}{d\Delta n}\frac{n_{i^2}}{\tau_{corr}} \ll \frac{d}{d\Delta n}\frac{n_{i^2}}{\tau_{SRH}} \quad (16)$$

Then Eq. (15) can be simplified as follows;

$$J_o = \frac{qW}{2}\frac{d}{d\Delta n}\frac{n_{i^2}}{\tau_{corr}} \quad (17)$$

At the present time, this equation is widely used in WCT-120 lifetime measurement instruments. More information regarding the measurement technique can be found in Kane and Swanson (1985), Sinton Instrument (2011), Sinton and Cuevas (1996), Kerr et al. (2002).

4. Experimental approach

Two different passivation schemes are investigated as follows: silicon rich oxy-nitride ($SiriO_xN_y$) capped with a PECVD-SiN_x layer, and thin thermally grown oxide, capped with a PECVD-SiN_x layer.

To evaluate the quality of a diffused surface, the dark saturation current density (J_o) is measured in high injection conditions (excess carrier concentration is bigger than doping density, $\Delta n \gg N_A$) by applying the quasi steady state photo conductance (QSSPC) technique.

The samples used in this experiment are monocrystalline *p*-type samples fabricated by the Czochralski method (C_z). The base is doped by Boron. The wafers are square with a dimension of 156×156 mm^2 and a thickness around 210 μm.

In total, 184 samples were fabricated in order to have enough samples for all the needed analysis that are explained in the following paragraphs.

The experimental procedure presented in this paper is shown in Fig. 2. The wafers are divided into two groups in order to apply a random pyramid texturize and alkaline saw damage etch, respectively.

Then all wafers are divided into four groups in order to apply the four industrial $POCl_3$ diffusion processes. At this point, the emitter region has being fabricated with different surface dopant concentration which depends on the applied diffusion process.

In order to obtain the phosphorus diffusion profile, 32 samples are selected to perform the ECV measurements on them for four different emitters with the recipe B, C, D and E. Because this is a destructive procedure, the samples used in this characterization technique cannot be further analyzed. The remaining samples (152) are then etched-back (at the emitter region) in an acidic bath of ozone applying four different time intervals (3, 5.3, 8 and 10.3 min) in order to control the etching depth (≈50–250 nm).

The samples are then divided into three groups in order to apply different passivation layers (SiO_x and SiriON) on both of the surfaces (these samples are called symmetrical lifetime samples) and then the QSSPC measurement is performed.

From the obtained minority carrier lifetime, the emitter dark saturation current density (J_o) can be calculated for both, planar (alkaline saw damage etch samples) and textured (random pyramid texturize samples) surfaces.

5. Results and discussions

5.1. Diffusion analysis on emitter homogeneity

The inhomogeneity of the diffusion for one wafer is defined here as the standard deviation of the sheet resistances of all measurement points for one single wafer. Basically, the sheet resistance (R_{sh}) differs on textured and planar surfaces over the wafer and is significantly higher on textured surface as shown in Fig. 3. This is expected due to the higher surface area in textured surface for the silicon ⟨111⟩ planes and because there is a significant amount of gas deposition variation over the wafer due to the high surface roughness. For further calculations, the textured and planar surface samples are considered separately (e.g. the calculation of the etch depth from the ECV profile taking into account textured and planar surface individually). Further characterization techniques (e.g. QSSPC, ECV, R_{sh}, etc.) are focused on the center of the wafer.

6. Recombination properties analysis

6.1. J_o values measurement for QSSPC analysis

Multiple samples signifies a linear behavior between the applied recombination value "n_i^2/τ_{orr}" and the injection density "Δn" (Fig. 4) from this behavior, the dark saturation current density J_o can be calculated as explained in Section 3.1. The uncertainty of the J_o values is then calculated by adding this error to the commonly assumed uncertainty of 10%. An additional measurement uncertainty is considered between the obtained J_o values from the low and high injection range (±3%).

The measurement graph shows a reasonable linear behavior. The measurement is independent of injection density which can be appreciated by comparing the graph which comprises of the high injection (green[1] line) and low injection (red line) regions.

6.2. J_o values measurement for SiriON passivated samples

The dark saturation current densities (J_o) measured over the sheet resistance of SiriON passivated and phosphorous diffused emitters are shown in Fig. 5. In this experiment, a promising industrial SiriON passivation layer for the emitter passivation has been investigated.

The error bars denote inhomogeneity of different samples and measurement uncertainties. The range of the sheet resistance is covered from 48 to 1578 Ω/sq.

The J_o values increase as the sheet resistance decreases. This is because, as the carrier concentration increases, the sheet resistance goes down (because there are more free carriers) and at the same time the Auger recombination increases which lead to an increase of J_o.

After the contact firing, the J_o values are as low as 7–9 fA/cm^2 while the measured sheet resistances are obtained in a range of 840–97 Ω/sq respectively. The lowest J_o values (≈7 fA/cm^2) for random pyramid textured samples passivated with SiriON has been measured for lightly doped emitters while the highest J_o values (≈156 fA/cm^2) are measured for industrial like emitters as the sheet resistance decreases from 840 to 55 Ω/sq. as shown in Fig. 5.

The lowest J_o values (≈8.5 fA/cm^2) for planar samples and passivated with SiriON has been measured for lightly doped emitters and the highest J_o values (≈123 fA/cm^2) are obtained for industrial like emitters as the sheet resistance decreases from 1578 to 48 Ω/sq as shown in Fig. 5. This is also consistent with the increase in surface area by a factor of 1.6 compared to planar surface. The J_o value is lower for shallow and lightly doped emitters.

It appears that the ratio of J_o for textured surface and planar surface of the same sheet resistance value increases as the sheet resistance increases. This result shows the good SiriON passivation quality for different surface morphologies.

6.3. J_o values measurement for thermal oxide (SiO_x) passivated samples

The measured dark saturation current densities value (J_o values) over sheet resistance of thermal oxide (SiO_2) passivated and

[1] For interpretation of color in Figs. 4 and 6, the reader is referred to the web version of this article.

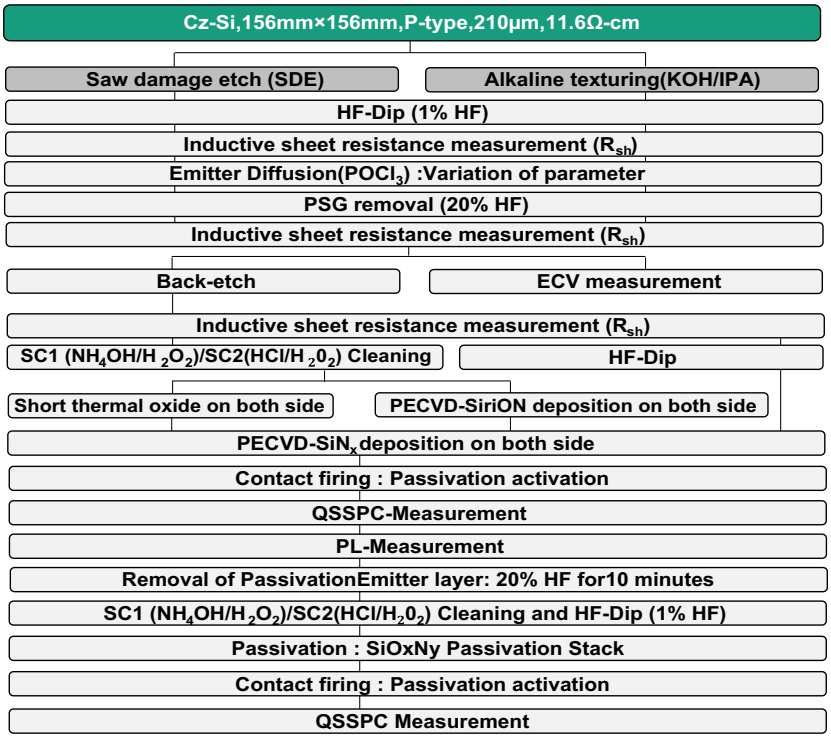

Fig. 2. Experimental procedure for the measurement of dark saturation current density.

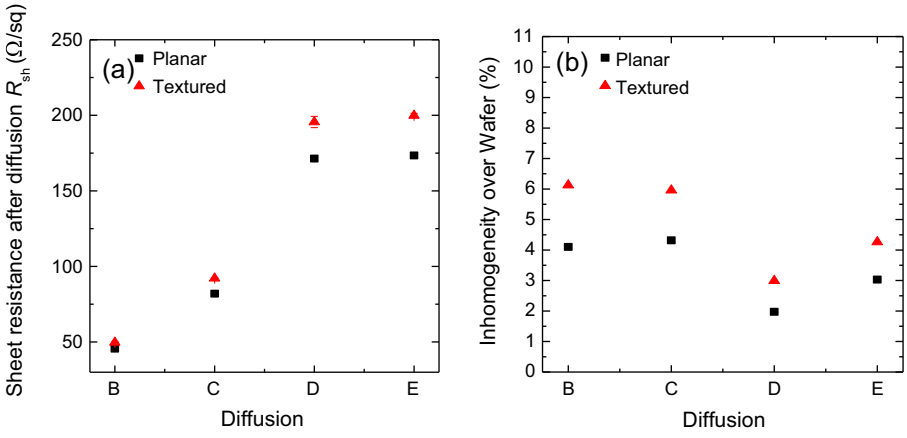

Fig. 3. (a) Measurement of the sheet resistance over different diffused emitter recipes. Sheet resistance of textured surfaces is always higher than the one of planar surfaces. (b) Inhomogeneity (standard deviation of all measurement points for one wafer) over the different diffused emitter recipes shows that planar surfaces exhibits lower deviation than textured surface.

phosphorous diffused emitters are shown in Fig. 6. The range of the sheet resistance is covered from 52 to 1239 Ω/sq, where the dark saturation current density (J_o) decreases with an increase of the sheet resistance (R_{sh}) as explained in the previous section.

As preferred, the J_o value increases as the sheet resistance decreases. J_o values as low as 3–6 fA/cm^2 have been measured for lightly doped emitters and as high as 90–160 fA/cm^2 for industrial like emitters. The J_o values for random pyramid textured samples passivated with thin thermal oxide and PECVD SiN_x are shown in Fig. 6. Values as low as 13 fA/cm^2 have been measured for lightly doped emitters and as high as 130 fA/cm^2 for industrial like emitters are obtained as the sheet resistance decreases from 780 to 60 Ω/sq, respectively.

The lowest J_o values (≈3 fA/cm^2) of planar samples have been measured for lightly doped emitters while the highest values (≈94 fA/cm^2) for industrial like emitters as the sheet resistance decreases from 854 to 52 Ω/sq as shown in Fig. 6. Furthermore, while the silicon rich oxy-nitride (SiriON) offers a good passivation quality, a thermal oxide (SiO_x) offers a superior passivation quality as mentioned in Sections 6.2 and 6.3. Comparing the data for textured and planar samples in Fig. 6, it is revealed that the J_o values increase for thermal oxide passivated surface when going from planar to a textured surface which is distinguished by a red and a blue sparse region. This is not observed for the SiriON.

7. Conclusion

In this experiment, the analysis of the recombination losses at the surface in dependence with the doping concentration and the passivation layer quality is presented. For this, samples with the same base properties but with different surface concentrations

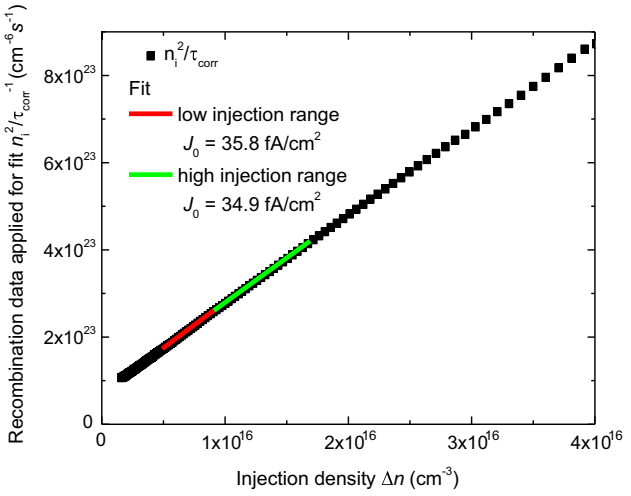

Fig. 4. Recombination value (n_i^2/τ_{orr}) versus injection density (Δn).

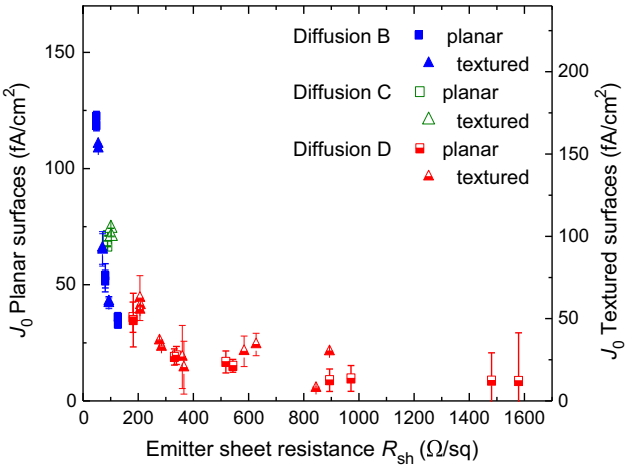

Fig. 5. Measured dark saturation current densities (J_o values) over sheet resistance of the SiriON passivated and phosphorous diffused emitters with a planar and textured surface. The measurement values for the textured samples are scaled up on the right hand side with a factor of 1.6 because the textured surface exhibits a higher surface area than the planar surface which affects the J_o calculation, so it is necessary to scale it up for the same range of comparison.

(1.3×10^{19} cm^{-3}, 9.3×10^{19} cm^{-3}, 1.9×10^{20} cm^{-3} and 2.8×10^{20} cm^{-3}) and profile depths (up to 750 nm) were prepared.

The sheet resistance measurement of the wafers showed a significant inhomogeneity of the emitters over the wafers. Thus all further characterization is referred to the center of each wafer.

The emitter doping profile is measured by applying the electrochemical-capacitance voltage (ECV) technique. Near the surface, a measurement artifact occurred leading to uncertainties of the obtained surface doping concentrations. Therefore, a result of the etch-back procedure is a significantly higher precision in measured surface concentration due to the avoidance of the surface near artifact by measuring the non-etched back profiles and obtaining the actual profile from the calculation of the etch depth.

The dark saturation current density of phosphorus-diffused surfaces is obtained for two different industrial passivation layers (SiriON and SiO_x). The consideration of the relation between J_o and sheet resistance shows that both the SiriON and SiO_x layers present good results (when the sheet resistance increases, the dark saturation current density decreases). For most samples, the ratio between the J_o on textured samples and planar samples seems to be 1.6, as preferred due to the ~1.6 time's higher surface area.

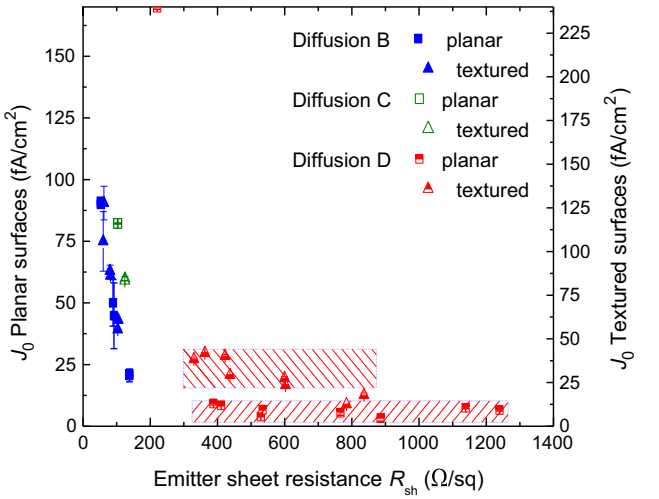

Fig. 6. Measured dark saturation current density (J_o values) over sheet resistance of the thermal oxide passivated and phosphorous diffused emitters with a planar and textured surface.

For thermal oxide passivated samples with low surface concentrations however, the $J_o/1.6$ of the textured surface exceeds J_o of the planar surface as mentioned in Section 6.3. This could be attributed to a higher defect density at the ⟨111⟩ surfaces of the textured samples than on the ⟨100⟩ surfaces of the planar surfaces. This effect was not visible for the SiriON passivated samples.

It is also demonstrated that both passivation layers present good surface passivation qualities on the $POCl_3$ diffused surfaces. As explained in Section 6, the SiriON and thermal oxide passivation techniques exhibit a reasonable low dark saturation current density even for the case of a high surface concentration. The results obtained in this thesis can be used to determine the surface recombination velocity for SiriON and SiO_x passivation stacks for a range of phosphorus surface concentrations of $5 \cdot 10^{18}$ cm^{-3} to $2.6 \cdot 10^{20}$ cm^{-3} for alkaline textured and planar surfaces.

Acknowledgements

I would like to express my deep appreciation and gratitude to Prof. Dr. Ulrich Herr, Prof. Dr. Hans-Jörg Fecht, Dr. Achim Kimmerle, Dr. Sebastian Mack and Sabrina Werner for enlightening me the first glance of research. I would like to thank of my fellow lab mate and friends Carlos Rodrigues, all co-authors and co-workers within the dispensing project as well as our industry partners and last but not least Fraunhofer Institute for Solar Energy Systems (ISE), Germany.

References

Baruch, P., De Vos, A., Landsberg, P.T., Parrott, J.E., 1995. On some thermodynamic aspects of photovoltaic solar energy conversion. Sol. Energy Mater. Sol. Cells 36 (2), 201–222.
Cuevas, A., Merchán, R., Ramos, J.C., 1993. On the systematic analytical solutions for minority-carrier transport in nonuniform doped semiconductors: application to solar cells. IEEE Trans. Electron Dev. 40 (6), 1181–1183.
Durán, J.C., Venier, G., Weht, R., 1991. Optimization of the junction depth and doping of solar cell emitters. Sol. Cells 31 (6), 497–503.
Kane, D.E., Swanson, R.M., 1985. Measurement of the emitter saturation current by a contactless photoconductivity decay method. In: IEEE Photovoltaic Specialists Conference, vol. 18.
Kerr, M.J., Campbell, P., Cuevas, A., 2002. Lifetime and efficiency limits of crystalline silicon solar cells. In: Photovoltaic Specialists Conference, 2002. Conference Record of the Twenty-Ninth IEEE. IEEE, pp. 438–441.
Luke, K.L., Cheng, L.J., 1987. Analysis of the interaction of a laser pulse with a silicon wafer: determination of bulk lifetime and surface recombination velocity. J. Appl. Phys. 61 (6), 2282–2293.

Nagel, H., Berge, C., Aberle, A.G., 1999. Generalized analysis of quasi-steady-state and quasi-transient measurements of carrier lifetimes in semiconductors. J. Appl. Phys. 86 (11), 6218–6221.
Powell, D.M., Fenning, D.P., Hofstetter, J., Lelievre, J.F., Cañizo Nadal, C.D., Buonassisi, T., 2012. TCAD for PV: a fast method for accurately modelling metal impurity evolution during solar cell processing. Photovoltaics Int. 15, 91–98.
Sinton, R.A., Cuevas, A., 1996. Contactless determination of current–voltage characteristics and minority-carrier lifetimes in semiconductors from quasi-steady-state photoconductance data. Appl. Phys. Lett. 69 (17), 2510–2512.
Sinton Instrument, U., 2011. WCT120-Photoconductance Lifetime Tester User Manual.
Sproul, A.B., 1994. Dimensionless solution of the equation describing the effect of surface recombination on carrier decay in semiconductors. J. Appl. Phys. 76 (5), 2851–2854.
Stangl, R., Leendertz, C., Haschke, J., 2010. Numerical Simulation of Solar Cells and Solar Cell Characterization Methods: The Open-Source on Demand Program AFORS-HET. InTech Open Access Publisher.
Sze, S.M., 1981. Physics of Semiconductor Devices, second ed. John Wiley & Sons, Inc., New York, NY, USA, p. 868.